Research Report

96-28

Modeling and Simulation of Matrix Converter/Induction Motor Drive

T. Matsuo, S. Bernet, R.S. Colby*, T.A. Lipo

Wisconsin Power Electronics
Research Center
University of Wisconsin-Madison
Madison WI 53706-1691

*Otis Elevator Company
5 Farm Springs Rd
Farmington CT 06032

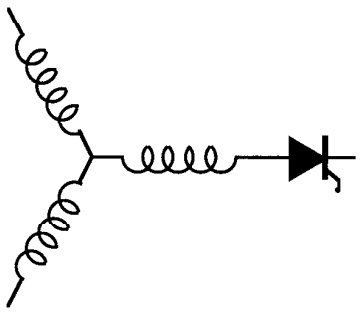

Wisconsin
Electric
Machines &
Power
Electronics
Consortium

University of Wisconsin-Madison
College of Engineering
Wisconsin Power Electronics Research Center
2559D Engineering Hall
1415 Engineering Drive
Madison WI 53706-1691

MODELING AND SIMULATION OF MATRIX CONVERTER/ INDUCTION MOTOR DRIVE

Takayoshi Matsuo, Steffen Bernet, R. Stephen Colby* and Thomas A. Lipo

University of Wisconsin-Madison
Electrical and Computer Engineering
1415 Johnson Drive
Madison, Wisconsin 53706
U. S. A.

*Otis Elevator Company
Five Farm Springs
Farmington, Connecticut 06032
U. S. A.

Abstract–Modeling and simulation of a matrix converter/induction motor drive are presented in this paper, which includes a three phase ac to ac matrix converter, an induction motor, a field oriented controller, filters and a power source. In addition, a developed precise loss calculation model for power converters is described with calculation results when it was applied to the matrix converter. A harmonic analysis is described with a developed switching strategy, which reduces the harmonic current at the matrix converter input.

1. INTRODUCTION

The ac to ac matrix converter was first investigated by Gyugyi and Pelly in 1976 [1]. More recently Venturini and Alesina have introduced a matrix converter design using a generalized high frequency switching strategy [2]. The matrix converter has recently attracted numerous researchers because of its simple topology, absence of large dc link capacitor, and easy control of input power factor. The purpose of this paper is to investigate via simulation the technical issues of applying the matrix converter to field oriented induction motor drives. In addition to the implementation of the drive system, a precise loss calculation model for power converters is described and applied to the drive system to study the loss characteristics of the matrix converter. The harmonic analysis of the matrix converter input current, the filter current, and the input power source current were performed to study the filter size and to develop a switching sequence combination which minimizes the harmonic contents of the matrix converter input current.

The simulation language ACSL [3] (Advanced Continuous Simulation Language) was used for this study, which is designed for modeling and evaluating the performance of continuous system described by time dependent, nonlinear differential equations and/or transfer functions. The language consists of a set of arithmetic operators, standard functions, a set of special ACSL statements, and a Macro capability.

2. MATRIX CONVERTER/INDUCTION MOTOR DRIVE

A three phase ac-ac matrix converter basically consists of a 3 x 3 switch matrix. The 9 bi-directional voltage blocking, current conducting switches are arranged so that any input phase can be connected to any output phase at any time. The 3 x 3 switch matrix can be arranged in the form of Fig. 1 for purpose of analysis. Since an inductive load is assumed, the voltage sources of the input must be created by placing capacitors (filter) from line to line across the converter input phases. In principle, for a given set of input three phase voltages, any desired set of output voltages can then be synthesized by suitably toggling the matrix switches.

Figure 2 shows a drive configuration for a field oriented control of an induction motor which is driven by a three phase to three phase matrix converter. By means of an incremental encoder or resolver, the angular position of the rotor θ_r is established. The angular position of the slip θ_s, which is calculated in the field oriented control module, is added to the angular position of the rotor θ_r to form the angular position of the stator MMF θ_e. These sinusoidal components are used to refer those physical stator currents from the physical (stationary) reference frame to the synchronously rotating (d-q) axes. The encoder is also used to measure speed. The voltage command signals from the field oriented controller are fed into the matrix converter block, where the matrix converter generates three phase PWM voltage pulses to drive the induction motor.

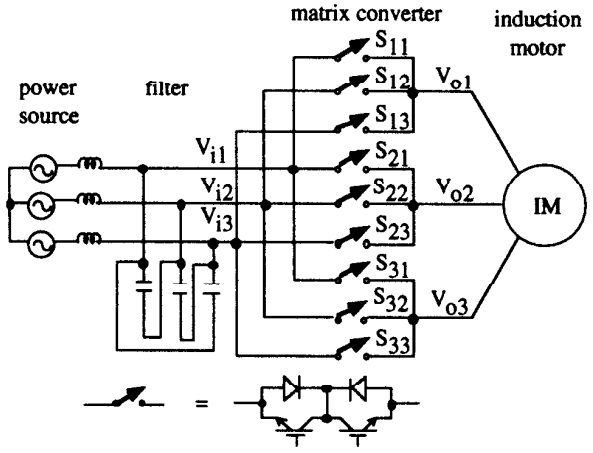

Fig. 1 Three phase ac to ac matrix converter.

3. THREE PHASE AC/AC MATRIX CONVERTER

Assuming that the voltages of the input are essentially constant during the switching interval, the average output voltage can be found during any switching interval by the equations

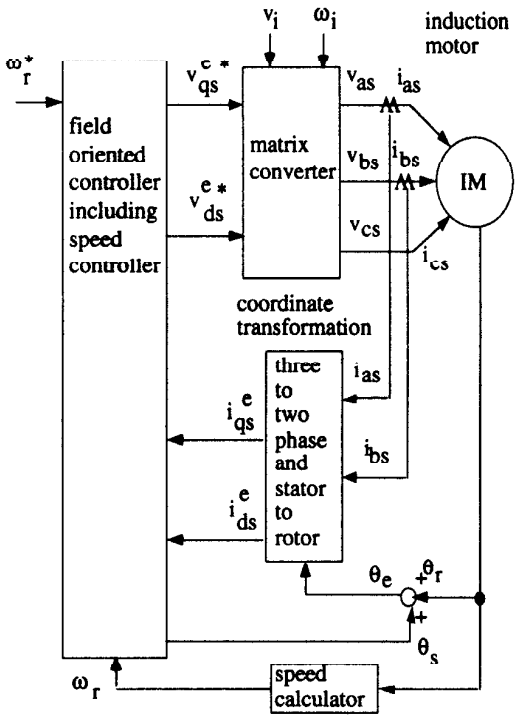

Fig. 2 Matrix converter/induction motor drive.

$$\frac{1}{T_s}\begin{bmatrix} V_{i1} V_{i2} V_{i3} \\ V_{i2} V_{i3} V_{i1} \\ V_{i3} V_{i1} V_{i2} \end{bmatrix}\begin{bmatrix} t_{1s} \\ t_{2s} \\ t_{3s} \end{bmatrix} = \begin{bmatrix} V_{o1} \\ V_{o2} \\ V_{o3} \end{bmatrix} \quad (1)$$

where

$$V_{iN} = V_I \cos(\omega_i t - (N-1)\, 2\pi/3) \quad (2)$$

$$V_{oN} = V_O \cos(\omega_o t + \theta_o - (N-1)\, 2\pi/3) \quad (3)$$

$$t_{1s} + t_{2s} + t_{3s} = T_s \quad (4)$$

N = 1, 2, and 3

where θ_o = arbitrary output voltage phase angle and T_s denotes the switching interval in seconds.

The three output voltages can also be synthesized by switching in the reverse direction such that during interval t_{1a}, phase a of the input is connected to phase a of the output, phase b of the input to phase c of the output and phase c of the input to phase b of the output. In effect the same output voltages can be generated except that the switches can be described by:

$$\frac{1}{T_s}\begin{bmatrix} V_{i1} V_{i2} V_{i3} \\ V_{i3} V_{i1} V_{i2} \\ V_{i2} V_{i3} V_{i1} \end{bmatrix}\begin{bmatrix} t_{1a} \\ t_{2a} \\ t_{3a} \end{bmatrix} = \begin{bmatrix} V_{o1} \\ V_{o2} \\ V_{o3} \end{bmatrix} \quad (5)$$

where

$$t_{1a} + t_{2a} + t_{3a} = T_s \quad (6)$$

Since the two switching strategies can produce exactly the same output voltage, in general, the output voltages can be formed by any combination of the symmetric (Eq. 1) and antisymmetric (Eq. 5) modes. That is,

$$\alpha_1 \frac{1}{T_s}\begin{bmatrix} V_{i1} V_{i2} V_{i3} \\ V_{i2} V_{i3} V_{i1} \\ V_{i3} V_{i1} V_{i2} \end{bmatrix}\begin{bmatrix} t_{1s} \\ t_{2s} \\ t_{3s} \end{bmatrix} + \alpha_2 \frac{1}{T_s}\begin{bmatrix} V_{i1} V_{i2} V_{i3} \\ V_{i3} V_{i1} V_{i2} \\ V_{i2} V_{i3} V_{i1} \end{bmatrix}\begin{bmatrix} t_{1a} \\ t_{2a} \\ t_{3a} \end{bmatrix} = \begin{bmatrix} V_{o1} \\ V_{o2} \\ V_{o3} \end{bmatrix} \quad (7)$$

where

$$\alpha_1 + \alpha_2 = 1 \quad (8)$$

It can be shown that while the output power factor angle ϕ_o is fixed by the load, the input power factor can be adjusted to any value consistent with Eqs. 9 and 10.

$$\alpha_1 = \frac{1}{2} + \frac{1}{2} \tan\phi_i \operatorname{ctn}\phi_o \quad (9)$$

$$\alpha_2 = 1 - \alpha_1 = \frac{1}{2} - \frac{1}{2} \tan(\phi_i) \operatorname{ctn}(\phi_o) \quad (10)$$

That is, if the power factor angle ϕ_o is given, then any value of ϕ_i can be chosen such that neither α_1 and α_2 are negative nor greater than one. That is, from inspection

$$-\phi_o \le \phi_i \le \phi_o \quad (11)$$

This equation demonstrates that the input power factor can always be made unity. In fact if the power factor is, for example, 60 degrees lagging, the input power factor can be adjusted to be as much as 60 degrees leading.

It should be noted that regardless of the switching strategy adopted, there are, however, physical limits on the output voltage achievable with this system. For complete control of the output voltage at any time, the envelope of the target output voltages must be wholly contained within the continuous envelope of the input voltages. This limit can be improved by adding a third harmonic at the input frequency to all target voltages [4]. The addition of this third harmonic increases the available output voltage range to 0.75 of the input when the third harmonic has a peak value of $V_I/4$. Further improvement of the transfer ratio can be achieved by subtracting a third harmonic at the output frequency from all target output voltages to minimize the range of the output voltage envelope to 0.866 of the peak phase voltage which allows an absolute maximum transfer ratio of 0.75/0.866 = 0.866 of V_I when this third harmonic has a peak value of $V_O/6$. Hence the maximum possible voltage transfer ratio becomes V_O/V_I = 0.75/0.866 = 0.866. A modulation strategy [M(t)] can be found such that [4]

$$[M(t)] \cdot [V_I(t)] = V_O \begin{bmatrix} \cos(\omega_o t + \theta_o) \\ \cos(\omega_o t + \theta_o - \frac{2\pi}{3}) \\ \cos(\omega_o t + \theta_o + \frac{2\pi}{3}) \end{bmatrix}$$

$$+ \frac{V_O}{2\sqrt{3}}\begin{bmatrix} \cos(3\omega_i t) \\ \cos(3\omega_i t) \\ \cos(3\omega_i t) \end{bmatrix} - \frac{V_O}{6}\begin{bmatrix} \cos(3\omega_o t + 3\theta_o) \\ \cos(3\omega_o t + 3\theta_o) \\ \cos(3\omega_o t + 3\theta_o) \end{bmatrix} = [V_O] \quad (12)$$

The switching periods $t_{ij}(t)$ are given by the equation

$$[T_{sw}(t)] = \begin{bmatrix} t_{11}(t) & t_{12}(t) & t_{13}(t) \\ t_{21}(t) & t_{22}(t) & t_{23}(t) \\ t_{31}(t) & t_{32}(t) & t_{33}(t) \end{bmatrix} = T_s\,[M(t)] \quad (13)$$

One can refer to Ref. 4 for the equations for [M(t)].

4. MATRIX CONVERTER MODEL

The implementation of the equations to calculate the switching periods $t_{ij}(t)$ for 9 bi-directional switches with the simulation language ACSL is straight forward because ACSL is a FORTRAN based language. The bi-directional switches are treated as ideal switches in the simulation program. The conditional switch function RSW, which is available in ACSL, was used to obtain voltage pulses which are associated with each switching interval. For example, to calculate the phase 1 output voltage, the corresponding ACSL instructions are

vo11 = RSW((ta.GT.0.0.AND.ta.LE.t11), vi1, 0.0) (14)

vo12 = RSW(tb.GT.0.0.AND.tb.LE.t12),vi2,0.0) (15)

vo13 = RSW(tc.GT. 0.0.AND.tc.LE.t13),vi3,0.0) (16)

The phase 1 output voltage is expressed as

vo1 = vo11 + vo12 + vo13 (17)

where tb = ta - t11 and tc = tb - t12. The instruction line of Eq. 14 means that the phase 1 output is connected to the phase 1 input for the time period from ta=0 to ta=t11, that is, vo11 = vi1 if 0.0 < ta < t11, otherwise vo11 = 0.0. The time ta is reset to zero at the beginning of each switching period T_s. The phase 2 and 3 output voltages can be calculated in the same manner.

vo21 = RSW((ta.GT.0.0.AND.ta.LE.t21), vi1, 0.0) (18)

vo22 = RSW(tc.GT.0.0.AND.tc.LE.t22),vi2,0.0) (19)

vo23 = RSW(td.GT. 0.0.AND.td.LE.t23),vi3,0.0) (20)

vo21 = RSW((ta.GT.0.0.AND.ta.LE.t31), vi1, 0.0) (21)

vo22 = RSW(te.GT.0.0.AND.te.LE.t32),vi2,0.0) (22)

vo23 = RSW(tf.GT. 0.0.AND.tf.LE.t33),vi3,0.0) (23)

The phase 2 and 3 output voltages are expressed as

vo2 = vo21 + vo22 + vo23 (24)

vo3 = vo31 + vo32 + vo33 (25)

where tc = ta - t21, td = tb - t22, te = ta - t31, and tf = te - t22.

Similar instructions are used to calculate input currents.

ii11 = RSW((ta.GT.0.0.AND.ta.LE.t11), io1, 0.0) (26)

ii21 = RSW((tb.GT.0.0.AND.tb.LE.t12), io1, 0.0) (27)

ii31 = RSW((tc.GT.0.0.AND.tc.LE.t13), io1, 0.0) (28)

ii12 = RSW((ta.GT.0.0.AND.ta.LE.t21), io2, 0.0) (29)

ii22 = RSW((tc.GT.0.0.AND.tc.LE.t22), io2, 0.0) (30)

ii32 = RSW((td.GT.0.0.AND.td.LE.t23), io2, 0.0) (31)

ii13 = RSW((ta.GT.0.0.AND.ta.LE.t31), io3, 0.0) (32)

ii23 = RSW((te.GT.0.0.AND.te.LE.t32), io3, 0.0) (33)

ii33 = RSW((tf.GT.0.0.AND.tf.LE.t33), io3, 0.0) (34)

The phase 1, 2 and 3 input currents are expressed as

ii1 = ii11 + ii12 + ii13 (35)

ii2 = ii21 + ii22 + ii23 (36)

ii3 = ii31 + ii32 + ii33 (37)

5. INDUCTION MOTOR MODEL

The simulation equations for an induction motor in the d-q stationary reference frame are typically described, for the q-axis stator winding, as [5]

$$\lambda_{qs} = \int \left(v_{qs} + \frac{r_s}{l_{ls}} (\lambda_{mq} - \lambda_{qs}) \right) dt \quad (38)$$

$$\lambda_{mq} = \frac{L_m^*}{l_{ls}} \lambda_{qs} + \frac{L_m^*}{l_{lr}} \lambda_{qr} \quad (39)$$

$$i_{qs} = \frac{\lambda_{qs} - \lambda_{mq}}{l_{ls}} \quad (40)$$

$$T_e = \frac{3}{2} \frac{P}{2} (\lambda_{ds}\, i_{qs} - \lambda_{qs}\, i_{ds}) \quad (41)$$

where

$$L_m^* = \frac{1}{\frac{1}{l_{ls}} + \frac{1}{l_{lr}} + \frac{1}{L_m}} \quad (42)$$

and λ denotes flux linkage, v and i denote voltage and current, respectively. Quantities with subscript q or d denote q-axis or d-axis quantities and quantities with subscript s or r denote stator or rotor quantities. r_s and r_r are stator and rotor resistance and ω_r is rotor speed. l_{ls} and l_{lr} are stator and rotor leakage inductances and L_m is the magnetizing inductance. T_e is the motor torque and P is the number of poles. Similar equations apply for the reamining d-q compoents [5].

The stator and rotor flux linkage equations are described in the form of integration, which is suitable for the simulation language ACSL. Equation 38 is described as Eq. 43 in ACSL.

lamdaqs = INTEG(vqs - rs*iqs, lamdaqs0) (43)

It is important to use the line to line voltage to perform the three phase to d-q coordinate transformation because each phase voltage of the matrix converter contains the third harmonic components to improve the output to input voltage ratio. The coordinate transformation equations to relate the matrix converter model to the induction motor model are,

$$v_{qs} = \frac{v_{abs} - v_{cas}}{3} \quad (44)$$

$$v_{ds} = \frac{-v_{bcs}}{\sqrt{3}} \quad (45)$$

where $v_{abs} = v_{o1} - v_{o2}$, $v_{bcs} = v_{o2} - v_{o3}$, and $v_{cas} = v_{o3} - v_{o1}$.

6. FIELD ORIENTED CONTROLLER MODEL

A field oriented controller based on d-q current controllers in synchronous reference frame is implemented. A typical d-q differential equation in synchronous reference frame is, [5]

$$v_{qs}^e = r_s\, i_{qs}^e + p\, \lambda_{qs}^e + \omega_e\, \lambda_{ds}^e \quad (46)$$

where

$$\lambda_{qs}^{e} = L_s i_{qs}^{e} + L_m i_{qr}^{e} \quad (47)$$

where quantities with the superscript e denote quantities in synchronous reference frame. The conditions of the field oriented control, which enable that the rotor flux vector has only one component λ_{dr}^{e} in the d-axis ($\lambda_{qr}^{e} = 0$), are described as

$$i_{qs}^{e*} = \frac{2}{3}\frac{2}{P}\frac{L_r}{L_m}\frac{T_e^*}{\lambda_{dr}^{e*}} \quad (48)$$

$$i_{ds}^{e*} = \frac{1}{L_m}\lambda_{dr}^{e*} + \frac{L_r}{L_m r_r} p\,\lambda_{dr}^{e*} \quad (49)$$

$$\omega_s^* = i_{qs}^{e*}\frac{r_r}{L_r}\frac{L_m}{\lambda_{dr}^{e*}} \quad (50)$$

Figure 3 shows a block diagram of a field oriented control of an induction motor including a speed controller. The required slip angular frequency ω_s to produce a specific motor torque is calculated based on the d-q current commands and motor parameters, which is shown in Fig. 4, and is integrated to obtain the slip angular position θ_s. Current regulators guarantee that the desired and actual values of the d-q currents are obtained. The voltage command signals which are obtained in the synchronously rotating d-q frame are, with the stator MMF angular speed, fed into the matrix converter block to produce PWM switching pulses for the matrix converter.

The exact nature of the speed invariant current control block is explained in Fig. 5. Referring to the stator voltage equations for an induction machine, Eq. 46 for example, the presence of the "counter emf terms" $\omega_e\lambda_{ds}^{e}$ and $\omega_e\lambda_{qs}^{e}$ is recalled. When speed changes rapidly, these terms cause an error in the current regulator since the integrators of the two PI current controllers must continually integrate at a rate proportional to speed due to the cemf terms in addition to performing their function of regulating the two components of stator current. This requirement can be eliminated by supplying the counter emf portion of the applied voltage separately by means of feed forward control as shown in Fig. 5. In this figure, the speed voltage components $\omega_e\lambda_{ds}^{e} = \omega_e L_m i_{ds}^{e} + \omega_e\sigma L_s i_{ds}^{e}$, and $\omega_e\lambda_{qs}^{e} = -\omega_e\sigma L_s i_{qs}^{e}$ are added to the outputs of the current regulators, $V_{qs}^{'*}$ and $V_{ds}^{'*}$ to form the applied voltages in the d-q frame, V_{qs}^{*} and V_{ds}^{*}, where $\sigma L_s = 1 - L_m^2/L_s L_r$.

The implementation of the field oriented controller into an ACSL simulation program is straight forward. PI controllers can be implemented with ACSL operators such as LIMINT. An ACSL statement described by Eq. 51 performs an integration of iqer*iqki with an initial value of vq0, a bottom bound on vqint of -vqmax, and a top bound on vqint of vqmax.

vqint = LIMINT(iqer*iqki,vq0,-vqmax,vqmax) (51)

7. INPUT FILTER AND POWER SOURCE MODEL

The three phase to three phase matrix converter is completed by filters at the input side. The output side filters can generally be omitted in motor drive applications, where the stator winding inductances of the motor work as the filters. One important role of the filters at input side is to keep the input voltage from changing significantly during each PWM cycle. Another important role is to absorb harmonic currents, which are generated by matrix converters, to prevent unwanted harmonic currents from flowing into ac main supplies and to satisfy any power quality regulation applicable.

A simple filter configuration was examined, as shown in Fig. 6, where a capacitor is connected between each line to line at the matrix converter input. The equations for one phase of the filter and power source are given as,

$$v_{s1} - v_{i1} = r\,i_{s1} + l_s\frac{di_{s1}}{dt} \quad (52)$$

$$i_{c1f} = i_{s1} - i_{i1} \quad (53)$$

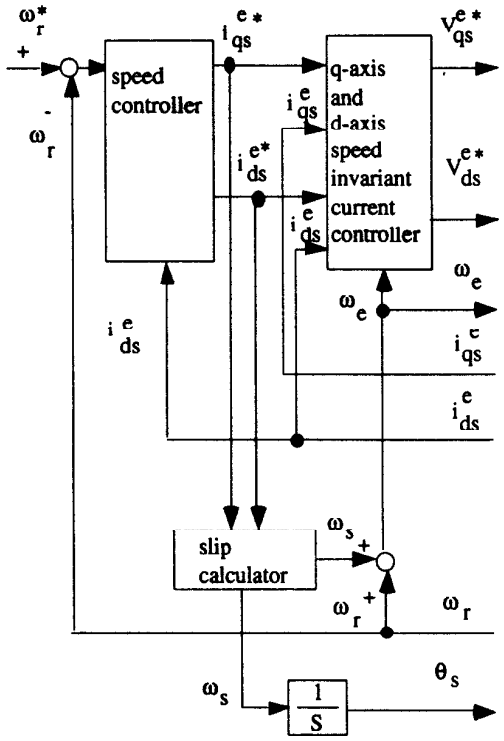

Fig. 3 A block diagram of a field oriented controller including a speed controller.

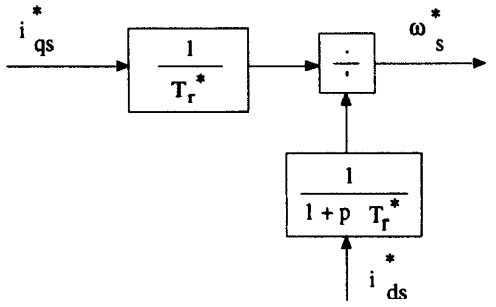

Fig. 4 Slip calculator.

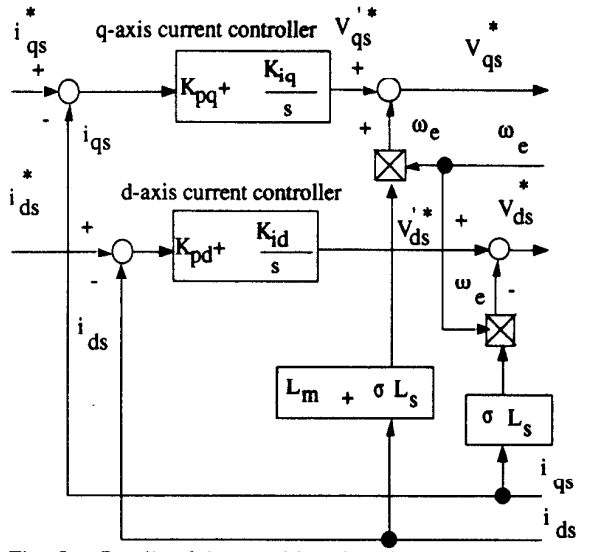

Fig. 5 Details of the speed invariant d-q current regulator.

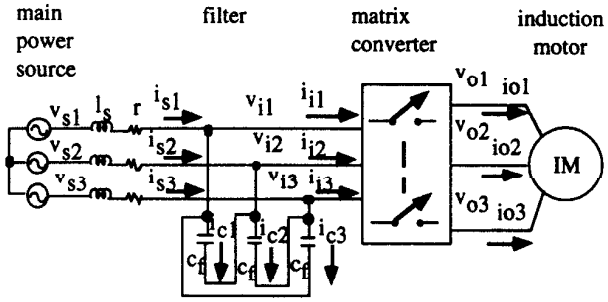

Fig. 6 Input filters and main power source of a matrix converter/induction motor drive.

$$i_{c1} = \frac{i_{c1f} - i_{c2f}}{3} \tag{54}$$

$$v_{c1} = \frac{1}{c_f}\int i_{c1}\, dt \tag{55}$$

$$v_{i1} = \frac{v_{c1} - v_{c3}}{3} \tag{56}$$

where l_s and r denote the leakage inductance and resistance of the power source and $v_{s1\sim3}$ are three phase source voltages. The remainder of the filter equations are apparent by symmetry.

8. SIMULATION RESULTS

To illustrate the use of these equations, a simulation was carried out with the input source line to line voltage of 480 V rms. The filter capacitance of 10 μF and the induction motor rating of 40 kW was used for this simulation run. A waveform of the phase a motor current and a filtered waveform of the phase a matrix converter output voltage are shown in Fig. 7. The matrix converter output voltage includes third harmonic components at both the input frequency and output frequency in addition to the fundamental component. Both third harmonic components do not appear on the line to line motor voltages because each matrix converter three phase output voltage has the same third harmonic component. Figure 8 shows a waveform of the phase a matrix converter output voltage for 3 msec. The wave form of v_{o1} in Fig. 7 is a filtered waveform of v_{o1} in Fig. 8. Typical waveforms of the voltage across one bi-directional switch and the switch current are presented in Fig. 9. Figure 10 shows how the capacitors at the matrix converter input work as the filters. Most of the harmonic components of the matrix converter input currents are absorbed into the filter capacitors. The voltage and current waveforms of the input main power source are shown in Fig. 11, where it is demonstrated that the input power factor is controlled at near unity value.

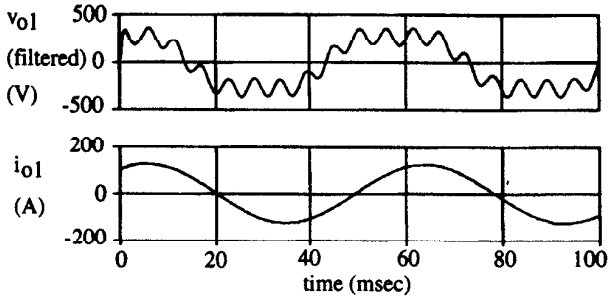

Fig. 7 A waveform of the phase a motor current and a filtered waveform of the phase a matrix converter output voltage showing added third harmonic components at both the input and output frequencies.

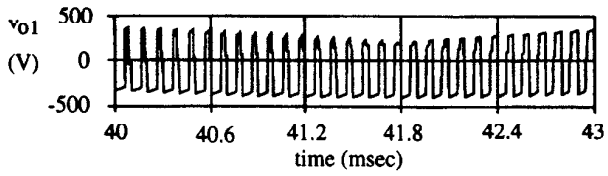

Fig. 8 A waveform of the phase a matrix converter output voltage.

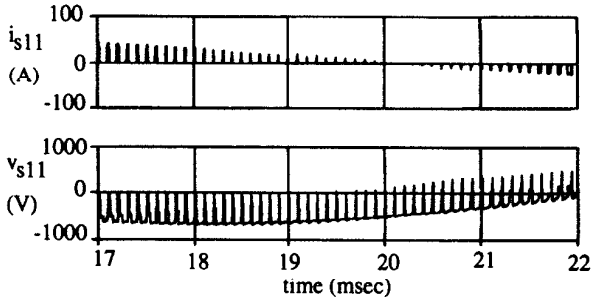

Fig. 9 Waveforms of the switch voltage and current, which is connected between the input phase 1 and the output phase 1.

The switching frequency of the matrix converter was set at 10 kHz, that is, the sampling interval of 100 μsec. The integration cycle in the ACSL program was set to carry out every 1 μsec.

9. HARMONIC CURRENT ANALYSIS

Harmonic components of the matrix converter input

currents, filter capacitor currents, and input source currents were analyzed to determine the size of the filter using the FFT (Fast Fourier Transformation) function in MATLAB. A numerical data file for each current/voltage is generated with ACSL program.

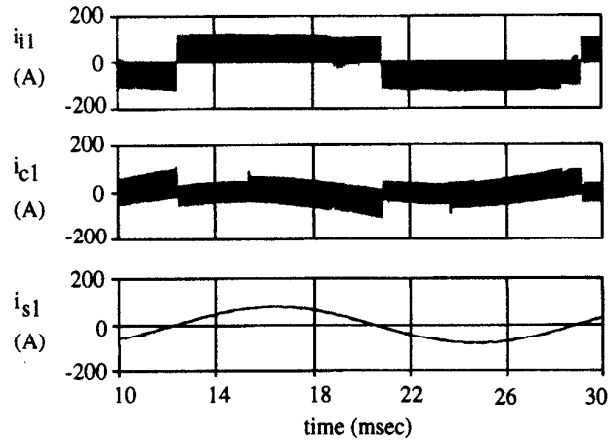

Fig. 10 Waveforms of the matrix converter input current, the filter capacitor current and the input current of the main power source.

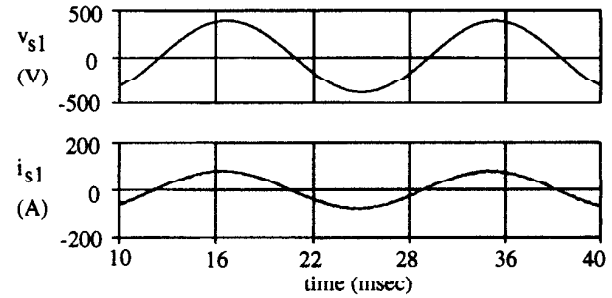

Fig. 11 Waveforms of the input voltage and current of the main power source.

Then, MATLAB processes the data for FFT. The ACSL program generates data points of waveforms every 1 μsec in the simulation described in Sec. 6. A FFT was performed for the data points of at least 1 cycle of output frequency, that is, when the output frequency is 10 Hz the data file has 100,000 points for 100 msec of data. MATLAB also calculates rms value and distortion index for each waveform and creates plot files for spectrum profiles. Typical spectrum profiles of the matrix converter input current, the filter capacitor current and the input power source current are shown in Fig. 12.

10. SWITCHING STRATEGY

An Optimized pulse pattern to minimize the input current harmonics, presented in Ref. 3, was implemented in the simulator for its switching strategy. Each output phase of a three phase to three phase matrix converter is connected to each three input phase for a certain time period during each switching interval. Each time period is determined so that each output

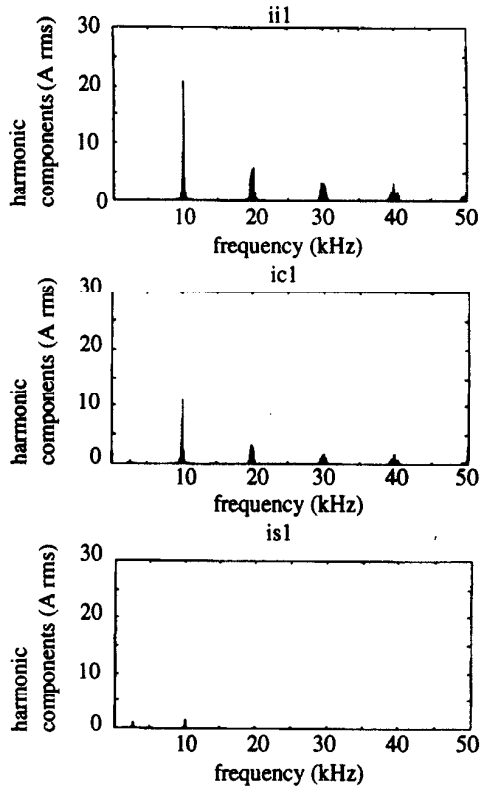

Fig. 12 Spectrum profiles of the matrix converter input current, the filter capacitor current, and the input source current.

voltage is to be an average voltage of three input voltage pulses.

$$v_{o1} = v_{i1} * \frac{t_{11}}{T_s} + v_{i2} * \frac{t_{12}}{T_s} + v_{i3} * \frac{t_{13}}{T_s} \quad (57)$$

$$v_{o2} = v_{i1} * \frac{t_{21}}{T_s} + v_{i2} * \frac{t_{22}}{T_s} + v_{i3} * \frac{t_{23}}{T_s} \quad (58)$$

$$v_{o3} = v_{i1} * \frac{t_{31}}{T_s} + v_{i2} * \frac{t_{32}}{T_s} + v_{i3} * \frac{t_{33}}{T_s} \quad (59)$$

The input phase 1 voltage appears in output phase 1 for a time interval t_{11}, the input phase 2 voltage for a time interval t_{12}, and the input phase 3 voltage for a time interval t_{13}, where $t_{11} + t_{12} + t_{13} = T_s$ and the switching interval $T_s = 1/f_s$ (f_s is the switching frequency). When the switching frequency f_s is 10 kHz the switching interval $T_s = 100$ μsec. There is no restriction on the sequence of the three time interval, that is, the output phase 1 can be connected to the input phase 2 first and then phase 3 and phase 1, or to the input phase 3 first and then phase 1 and phase 2. The output voltage v_{o1} remains same in either switching sequence combinations. There are basically 216 different switching sequence combinations for a nine-switch three phase to three phase matrix converter to produce specific three phase output voltages. Matrix converter input current characteristics depend on the switching sequence combinations while output current characteristics are not significantly affected by the change of the switching sequence combinations.

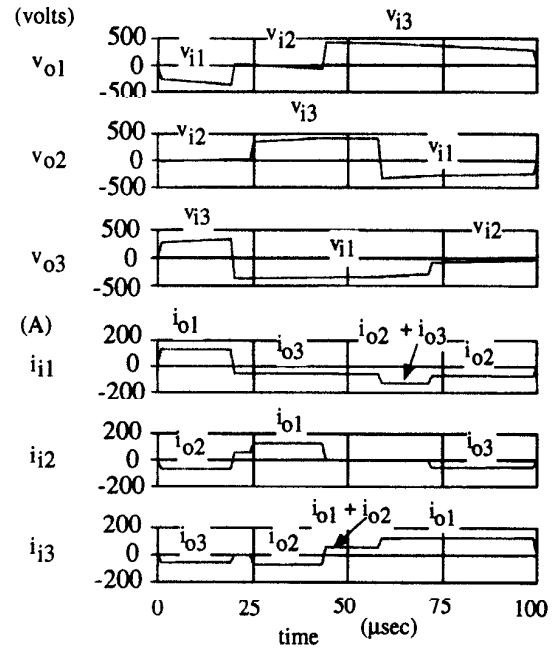

Fig. 13 Illustration of one of the switching sequence combinations showing waveforms of three phase output voltages and three phase input currents during one switching interval.

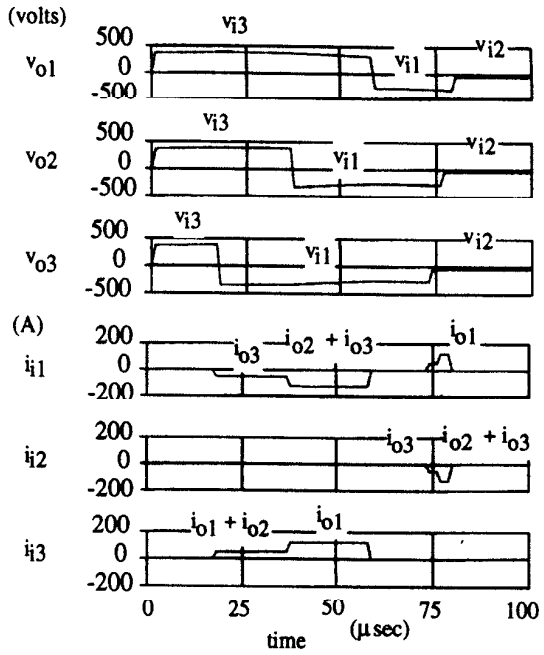

Fig. 14 Illustration of one of the switching sequence combinations, which reduces the harmonic components of the matrix converter input currents, showing waveforms of three phase output voltages and three phase input currents during one switching interval.

It was found [6] that the input current rms value can be reduced by applying proper switching sequence combinations, which increase the time period when all the three output phases are short circuited at the matrix converter input. The condition can be achieved by switching the three switches connected to the same input phase at the same time. The switching sequence combinations illustrated in Figs. 13 and 14 produce the same fundamental components for both output voltages and input currents. However, the total rms values of the phase 1, 2 and 3 input currents of Fig. 14 are 17%, 39%, and 39 % less than the ones of Fig. 13, respectively. There exist two other switching sequence combinations that produce minimum total rms values of the input currents, which are the alternative schemes to the one illustrated in Fig. 14. Balanced three phase input current can be obtained by alternating the three switching sequence combinations. Low alternating frequency keeps the lowest major harmonic components near the switching frequency.

11. SEMICONDUCTOR LOSS MODEL

The implementation of physical semiconductor models is often not possible or very inefficient in large systems to be simulated. This is especially the case in the drive system depicted in Fig. 1 where each of the nine forward and reverse blocking bi-directional current conducting switches is realized by a back to back arrangement of IGBTs (Common Collector Configuration [6]). Since each four-quadrant switch (4QSW) consists of 2 IGBTs and 2 diodes, the semiconductor losses of 18 IGBTs and 18 diodes have to be detected. To solve this problem at low computation time a semiconductor loss model has been developed which allows on the basis of ideal switching transients a sufficiently accurate loss estimation of each semiconductor. The loss model contains besides an analytical description of the significant losses especially an algorithm which determines the type of each occurring switching transient and distributes the losses to the active semiconductors (2 IGBTs, 2 diodes) of the switches.

The commutation of an output phase current from one switch to another in each of the three switch groups can be described by the equivalent commutation circuit presented in [7]. Two fundamental commutations can be distinguished according to the instantaneous power of the load- the inductive commutation with a positive gradient of power and the capacitive commutation with a negative gradient of power.

The inductive commutation is initiated by a hard turn-on transient of a 4QSW (IGBT) and completed by the passive turn-off transient of the other 4QSW (diode) during the interruption of the reverse current. In contrast to this the capacitive commutation is characterized by a hard turn off transient (IGBT) and a low loss passive zero voltage turn on transient (diode). Detailed investigations of the switching losses of hard switching 4QSWs showed that nearly all switching losses are caused by the active turn on transient of the IGBTs (W_{ONT}) as well as the reverse recovery losses of the diodes (W_{OFFD}) during the inductive commutation and the active turn off transient of the IGBTs (W_{OFFT}) during the capacitive commutation.

The basis of the model is the analytical description of these switching losses and the on-state voltages at junction temperatures of T_j=25°C and T_j=125°C approximated by the following equations:

$$v_{CE} = \left(v_{0T} + r_{0T} \cdot i_S^{\beta conT}\right) \cdot \left(1 - \frac{125°C - T_j[°C]}{100°C} C_{conT}\right) \quad (60)$$

$$v_D = \left(v_{0D} + r_{0D} \cdot i_S^{\beta conD}\right) \cdot \left(T_j[°C] - 125°C\right) \cdot C_{conD} \quad (61)$$

$$W_{ONT} = \left(A_{ONT} \cdot i_S^{B_{ONT}}\right) \left(1 - \frac{125°C - T_j[°C]}{100°C} C_{ONT}\right) \cdot F \quad (62)$$

$$W_{OFFT} = \left(A_{OFFT} \cdot i_S^{B_{OFFT}}\right) \left(1 - \frac{125°C - T_j[°C]}{100°C} C_{OFFT}\right) \cdot F \quad (63)$$

$$W_{OFFD} = \left(A_{OFFD} \cdot i_S^{B_{OFFD}}\right) \left(1 - \frac{125°C - T_j[°C]}{100°C} C_{OFFD}\right) \cdot F \quad (64)$$

$$F = \left(1 - \frac{600V - |v_C[V]|}{600V}\right) \quad (65)$$

where v_c: Commutation voltage
T_j: Junction temperature
v_o: Bias voltage at T_j=125° C
r_o: Dynamic resistance at T_j=125° C
A,B,C: Curve fitted constants at T_j=125° C, (v_c=600V)

The fitting of the on-state voltages and switching losses for IGBT and diode of the considered 1200V/300A NPT-IGBT module SKM400GA122D with "Mathematica" has produced the constants given in Table 1. It should be mentioned that the correspondence between the data contained in the data sheet and the fitted functions is excellent for both the on-state voltages and the switching losses of IGBT and diode (relative error 5%).

Figure 15 shows the flow chart of the implemented IGBT- and diode loss model for the switch group sg1 (S_{11},S_{12},S_{13}) of the matrix converter. Because the program parts of the other two switch groups are completely dual it is sufficient to discuss only the represented flow chart.

First, the state of all switches of the matrix converter is fixed to a starting position in the "Initial" section of the simulation program. Starting with the run of the integration algorithm in the "Derivative" section the values of the input voltages and output currents of the matrix converter are computed for each integration step Δt. The actual loss model begins with a renewed observation of the turned on switches and a determination of the switch currents on the basis of the current duty cycles. If the active switch was turned on with the new integration step initially, the type of the occurring commutation is determined by an analysis of the directions of the commutation voltage (voltage interval) and the load current [7]. Afterwards the turn on losses are computed corresponding to the current values of the switch current, the line to line voltage and the junction temperature. The distribution of the turn on losses to the semiconductors of a switch (which means the addition of the occurring turn on losses to the total turn on losses and the total semiconductor losses of the turning on device) is possible by an evaluation of the former state of the switches, the direction of the switch current and the type of the occurring commutation.

The following computation and distribution of the turn off losses of the occurring commutation is realized in exactly the same manner as in the case of the turn on losses with the only difference that the turn off losses are distributed to the IGBTs or diodes of the other two switches.

At the end of the detection of the switching losses the new state of the switches is set. After that (or immediately after the detection of the switch current if the switch was not turned on with the new integration step) the on-state voltages of the IGBT and the diode are computed for the current values of the junction temperature and the switch current.

Finally the resulting on-state losses are distributed according to the direction of the switch current to one IGBT and one diode and the losses are added to the total losses of the active semiconductors.

Since on the one hand the switching- and on-state losses are computed at each integration step and on the other hand also the fitted loss functions approximate the losses contained in the data sheet excellent, the realized loss model should describe accurately the semiconductor losses of a real matrix converter. Furthermore the semiconductor loss model is quite fast because only logical operations and some simple computations have to be carried out.

As an example, Fig. 16 shows the computed on-state voltages of the active IGBTs and diodes of the switch S_{11}. Obviously the minimum values of the on-state voltages- the bias voltages - are reached when the switch current becomes zero.

Figure 17 shows the waveforms of a variable which determines the type of the commutation of the load current from S_{11} to S_{12} (TR12=2 for capacitive commutations, TR12=-1 for inductive commutations) and the turn-off losses in the diode (W_{OFFD11}) and the IGBT (W_{OFFT11}) of S_{11} which carry the positive load current. It is to be seen that the turn off losses are generated in the transistor if there is a capacitive commutation and in the diode if an inductive commutation takes place.

Table 1 Fitted parameters of the NPT-IGBT module SKM400GA122D (1200V/300A) for loss calculation.

	IGBT	Diode
$v_{0T/D}$	0.55	0.4
$r_{0T/D}$	0.11	0.11
$B_{conT/D}$	0.55	0.49
$C_{conT/D}$	0.16	0.00396
A_{ONT}	0.18	
B_{ONT}	1.01	
C_{ONT}	0.36	
$A_{OFFT/D}$	0.49	0.22
$B_{OFFT/D}$	0.79	0.65
$C_{OFFT/D}$	0.165	0.69

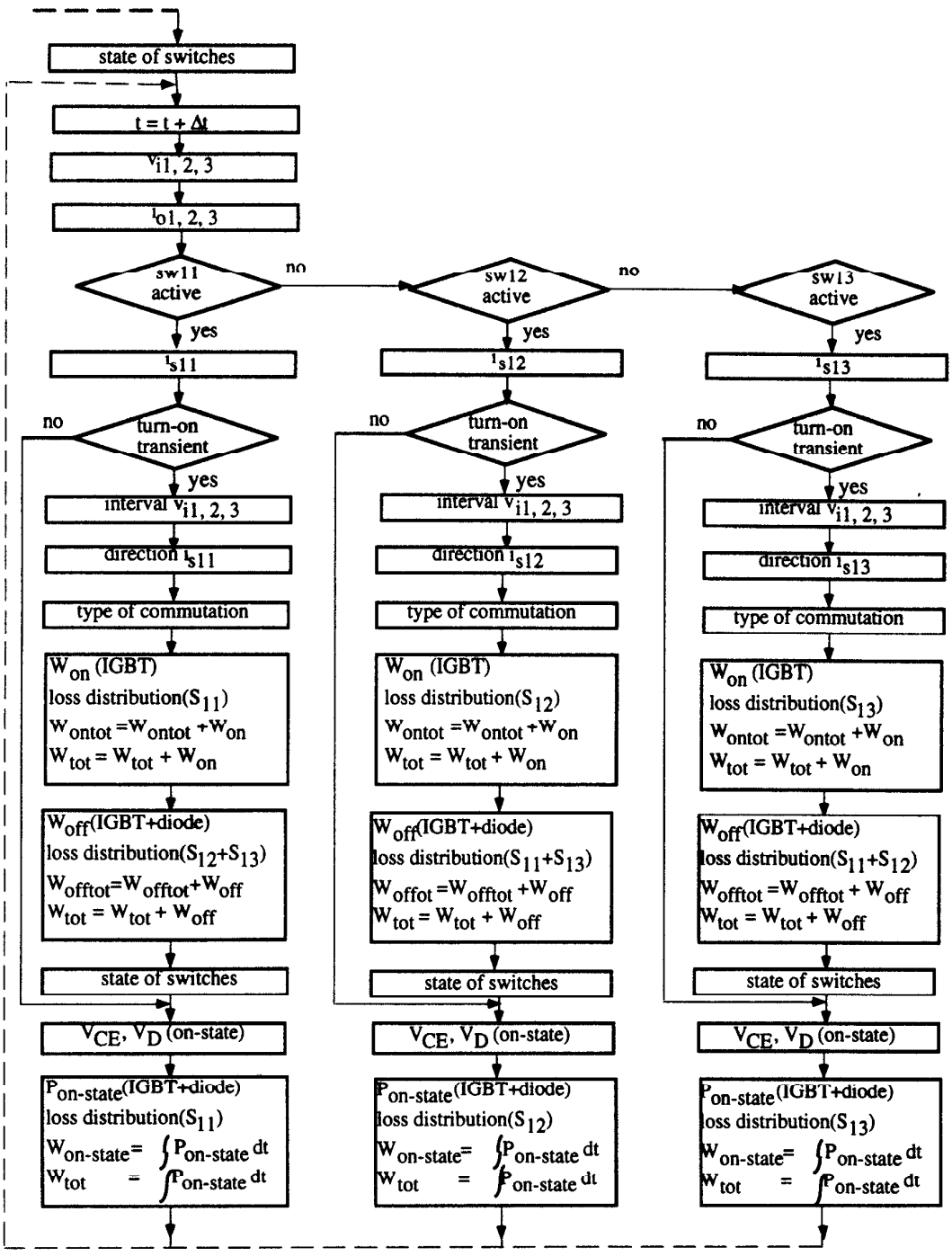

Fig. 15 Flow chart of the implemented semiconductor loss model for one switch group of the matrix converter.

12. ESTIMATED CONVERTER LOSSES

The function of the converter losses of the rated motor torque for three different speeds in Fig. 18 shows that the losses are strongly dependent on the torque which determines the load current. The decrease of the losses at high torques and high speed (e.g. 100% speed) is caused by the effective reduction of the switching frequency at the upper limit of the maximum output voltage of the converter. Fig. 19 shows the distribution of the total semiconductor losses for the IGBT and the diode of the switch S_{11} which carry the positive load current for different switching frequencies. The turn on-, turn off- and on-state losses of the IGBT at 10kHz are approximately the same for 100% rated

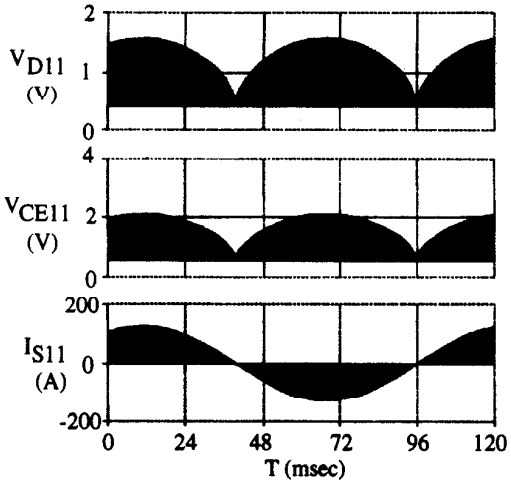

Fig. 16 On-state voltages and switch current of the switch S_{11} (SKM400GA122D; T_j=125°C; f_s=10kHz; ω=125rpm; T=100%).

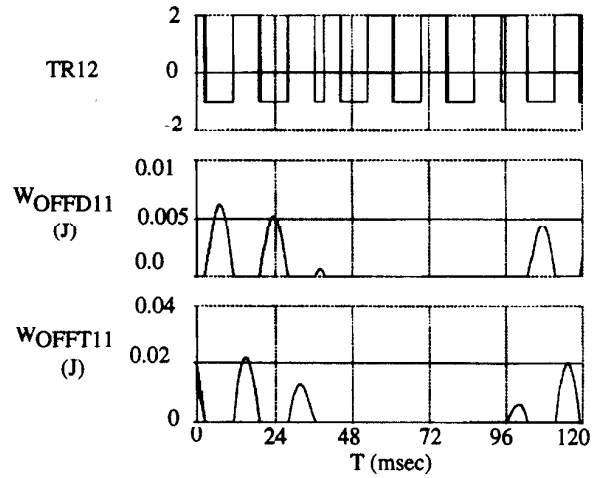

Fig. 17 Type of commutation and turn off losses of the IGBT and the diode of S_{11} which carry the positive load current (SKM400GA122D; T_j=125°C; f_s=10kHz; ω=125rpm; T=100%).

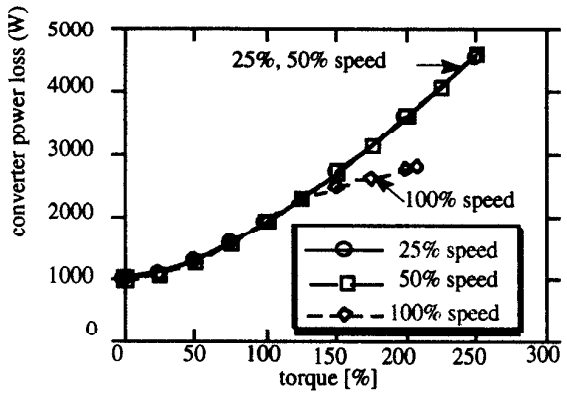

Fig. 18 Matrix converter losses versus the normalized motor torque for various speeds (SKM400GA122D; T_j=125°C; f_s=10kHz).

torque. However at high switching frequencies substantial switching losses arise which limit the converter efficiency essentially.

13. CONCLUSIONS

The implementation of the entire matrix converter/induction motor drive system into a simulation program was presented in this paper, which includes a three phase ac to ac matrix converter, an induction motor, a field oriented controller and a filter and a power source. In addition to the implementation of the drive system, a precise loss calculation model for power converters has been developed and applied to the drive system and the loss characteristics of the matrix converter were investigated. The harmonic analysis was shown to be a useful tool to develop a switching sequence combination which minimizes the harmonic contents of the matrix converter input current.

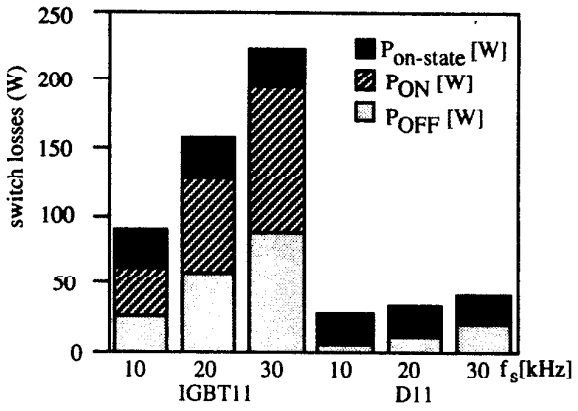

Fig. 19 Loss distribution of the IGBT and the diode of S_{11} which carry the positive load current (SKM400GA122D; T_j=125°C; f_s=10kHz; T=100%).

REFERENCES

[1] L. Gyugyi and B. R. Pelly, Static Power Frequency Changers. New York: Wiley-Interscience, 1976.

[2] A. Alesina and M. Venturini, "Solid state power conversion: A Fourier analysis approach to generalized transformer synthesis," IEEE Transactions on Circuit Systems, Vol. CAS-28, No. 4, 1981, pp. 319-330.

[3] ACSL Reference Manual, Mitchell and Gauthier Associates, Concord, MA, 1986.

[4] A. Alesina and M. Venturini, "Analysis and design of optimum-amplitude nine-switch direct ac-ac converters," IEEE Trans. on Power Electronics, Vol. 4, No. 1, Jan. 1989, pp. 101-112.

[5] D.W. Novotny and T.A. Lipo,"Vector Control and Dynamics of AC Drives" , Oxford Press, 1996 (to appear).

[6] S. Bernet, T. Matsuo, T.A. Lipo, "A Matrix Converter Using Reverse Blocking NPT-IGBTs and Optimized Pulse Patterns", Conference Record IEEE-PESC, Baveno, Italy, June 24-27, 1996, in progress.

[7] S. Bernet, "Power Semiconductors as ZCS in Soft Switching Power Converters", Ph.D. thesis, TU Ilmenau (Germany), 1995.